Evidence for Microbunching "Sidebands" in a Saturated Free-Electron Laser Using Coherent Optical Transition Radiation

A. H. Lumpkin, R. Dejus, J. W. Lewellen, W. Berg, S. Biedron,* M. Borland, Y. C. Chae, M. Erdmann, Z. Huang, K.-J. Kim, Y. Li, S. V. Milton, E. Moog, D. W. Rule,† V. Sajaev, and B. X. Yang

Advanced Photon Source, Argonne National Laboratory, Argonne, Illinois 60439

(Received 17 July 2001; revised manuscript received 26 November 2001; published 23 May 2002)

We report the first measurements of z-dependent coherent optical transition radiation (COTR) due to electron-beam microbunching at high gains ($>10^4$) including saturation of a self-amplified spontaneous emission free-electron laser (FEL). In these experiments the fundamental wavelength was near 530 nm, and the COTR spectra exhibit the transition from simple spectra to complex spectra (5% spectral width) after saturation. The COTR intensity growth and angular distribution data are reported as well as the evidence for transverse spectral dependencies and an "effective" core of the beam being involved in microbunching.

DOI: 10.1103/PhysRevLett.88.234801 PACS numbers: 41.60.Cr, 41.60.Ap

There is growing interest in the development of new light sources in the x-ray regime with improved spatial and spectral coherence properties compared to the present-day storage ring synchrotron radiation sources. One of the strongest candidate techniques at this time is the self-amplified spontaneous emission (SASE) free-electron laser (FEL) with a projected peak brightness improvement of $>10^{10}$ [1]. This would be accomplished by sending a high brightness electron beam through a long undulator magnet to generate synchrotron light. The SASE process relies on the longitudinal microbunching of the electron beam at the fundamental resonant wavelength as it interacts with the optical fields of the copropagating emitted synchrotron radiation and the magnetic field of the undulator. A favorable instability results in increasing numbers of electrons being involved in the microbunching and concomitantly stronger coherent light emission within the exponential gain regime [2–4]. This interaction of the optical mode with the microbunched part of the beam is particularly critical. We report in this Letter the z-dependent characterization of the microbunching using coherent optical transition radiation (COTR) techniques [5] that for the first time elucidate the evolution throughout the exponential gain regime *and* into the postsaturation regime. We present not only evidence for spectral "sidebands" in the COTR after saturation but also the correlated effect for the SASE radiation. Spectral quality is, of course, a fundamental property of any laser or laserlike source so its study is of high relevance to future SASE-FEL-based light sources. Spectral effects were discussed in the SASE exponential gain regime up to saturation in Ref. [6] and previously in terms of a FEL amplifier in Ref. [7]. We also report evidence of the transverse dependence of microbunching, the peaking of the COTR signal (microbunching) at/near saturation, and the subsequent "debunching" in the postsaturation regime. These unique COTR measurements have already resulted in an improved understanding of the SASE process and may be relevant to FEL amplifiers and inverse FEL-based laser acceleration schemes.

A brief discussion of the generation of COTR is in order. Coherent radiation by a bunch of electrons can be expressed as the product of a term representing the radiation process for a single particle and a term that takes into account how much of the charge radiates together, constructively in phase. Thus, the number of photons per unit frequency per unit solid angle can be expressed as $d^2W/d\omega d\Omega = [N + N(N-1)F(\mathbf{k})](d^2W_1/d\omega d\Omega)$ where

$$\frac{d^2W_1}{d\omega d\Omega} = \frac{4}{\pi^2}\beta^2\left(\frac{e^2}{\hbar c}\right)\frac{1}{\omega}\frac{\theta^2}{(\gamma^{-2}+\theta^2)^2} \times \sin^2\left[\frac{kL}{4}(\gamma^{-2}+\theta^2)\right], \quad \theta^2 = \theta_x^2 + \theta_y^2 \tag{1}$$

is the single-particle spectral, angular distribution for a two-foil optical transition radiation (OTR) interferometer [8,9]. The $\theta^2/(\gamma^{-2}+\theta^2)$ factor gives the angular lobe pattern of the single-foil OTR, and the $\sin^2$ term gives the fringe modulation due to interference of the OTR from the two surfaces. In these expressions N is the number of particles in the bunch, $F(\mathbf{k})$ is the square of the Fourier transform $[\mathcal{F}(\mathbf{k})]$ of the spatial distribution of the bunch, θ is the angle with respect to the beam direction, γ is the relativistic Lorentz factor, L is the separation of the two surfaces, ω is the frequency of the radiation with wave number $k = \omega/c$, e is the electron charge, $\hbar$ is Planck's constant over 2π, and c is the speed of light. When $F(\mathbf{k}) = 1$, there is an N^2 enhancement over the single-particle intensity, and the coherence is maximized. Using a Gaussian approximation for the beam distribution, with rms transverse sizes σ_x and σ_y and a longitudinal size σ_z, the transform function $\mathcal{F}(\mathbf{k}) = \rho(\mathbf{k})/Q$ is

$$\mathcal{F}(\mathbf{k}) = \frac{1}{(2\pi)^{3/2}} e^{-(\sigma_x^2k_x^2+\sigma_y^2k_y^2+\sigma_z^2k_z^2)/2}\frac{\sin(Mk_z\frac{\ell}{2})}{\sin(k_z\frac{\ell}{2})}, \tag{2}$$

where there are $M+1$ microbunches in a micropulse, each separated by a distance $\ell = \lambda_r$.

Microbunching causes the additional modulation in the longitudinal distribution that results in enhanced radiation at the fundamental wave number $k = k_r = 2\pi/\lambda_r$ and its harmonics $k_n = nk_r$, $n = 1, 2, 3, \ldots$, where the sine term in Eq. (2) has sharp maxima. The fraction of the micropulse, which radiates with wave number k_n, changes with distances z along the SASE FEL as the copropagating optical field (SASE light) increases the microbunching effect. The total number of emitted photons for forward COTR has been shown [10] to be proportional to $(Nb_n)^2$ and $(\gamma/nk_r)^4$, where b_n is the amplitude of the Fourier component of the electron distribution with spatial frequency k_n.

These experiments were performed with a significantly enhanced and altered accelerator and undulator configuration compared to our initial microbunching experiments. Our first experiments used an rf thermionic gun with an α magnet, while the present experiments use a photocathode (PC) rf gun and a chicane bunch compressor. In addition, the undulator string was increased from five to nine undulators for a total undulator magnetic length of 21.6 m. With this new configuration, our SASE FEL showed high gain and saturation near 530 and 385 nm, as reported elsewhere [6]. Our augmented FEL facility is schematically shown in Fig. 1. The PC gun provided more charge per micropulse and improved emittance compared to the rf thermionic gun used in our first experiment. The frequency quadrupled ND:glass laser pulse with a length of 4 ps (FWHM) was directed onto the Cu photocathode of the gun to generate micropulses with about 150–200 pC of charge at 6 Hz [11]. The beam was accelerated to 150 MeV, and the single micropulse was bunch compressed in the chicane to provide peak currents from 250–300 A [12]. The beam was accelerated to its final 217 MeV and the energy/energy spread was measured in an electron spectrometer. The final bunch length of 0.2 to 0.3 ps (rms) was also measured using the zero-phasing rf technique at the final linac structure and with transport into this same spectrometer. The transverse emittance of the beam was measured with a three-screen emittance technique to be $(7-9)\pi$ mm mrad, normalized. The beam was then transported to the low-energy undulator test line (LEUTL) tunnel [6], where a set of nine undulators was installed.

The optical diagnostics stations [13] before the first and after each of the undulators consists of a YAG:Ce converter, mirror, and thin-foil position on an actuator with a camera viewing the YAG:Ce scintillator denoted as Y0-Y9. A second removable 45° mirror is located 63 mm downstream of each YAG (yttrium-aluminum-garnet) actuator. When this mirror is inserted, another set of visible light detector (VLD) cameras is used to view either undulator radiation (UR) or COTR (when the 6-μm-thick foil upstream is inserted). Both near-field focus and far-field focus configurations were possible to provide beam profile and radiation angular distribution information, respectively. Since the spacing between the foil and the second metal mirror is on the order of the vacuum coherence length $L_v = \gamma^2\lambda \approx 14$ mm, we actually see interference phenomena in the COTR signals analogous to previously reported OTR interference patterns [5,8,14]. In addition, another set of flippable mirrors and lens pairs provides a relay path from each station to an in-tunnel Oriel M257 UV-visible spectrometer. A schematic of the stations is shown in Fig. 2 of Ref. [5]. The basic experiments involved the acquisition of digital images of the UR after each of the nine undulators. After demonstrating that there was significant z-dependent intensity growth in the UR, the COTR data were recorded by inserting the thin foil and the second 45° mirror at each station in sequence. Since the gain appears to saturate in the U5 to U7 regime, we obtained the critical intensity, spectral, and angular distribution data before, at, and beyond saturation (for the first time for COTR).

Figure 2 shows one of the fundamental SASE measurements, the z dependence of the UR and the COTR optical energy. All the experimental curves show the saturated gain effect. The error bars use the 25th and 75th percentiles of the optical intensity. The latter shows less variance after saturation in all four cases. In Fig. 2a the exponential gain regime extends from approximately 5 to 15 m. Both the UR (Δ) and the COTR ($\square$) show significant relative gains of 10^4 to 10^6 at 15 m as compared to the 2.4-m point. The UR radiation is approximately 1000 times stronger than the COTR intensities in this regime. In Fig. 2b, saturation occurred at 12.5 m, and after that the microbunching evidently decreases based on the COTR intensities. This decrease is not seen in the complementary UR data because all the light in the vacuum chamber bore is measured, including significant contributions from the last one or two gain lengths. However, COTR data are generated/sampled at the discrete z location of the blocking foil and mirror. In this sense the COTR experiment is a more definitive

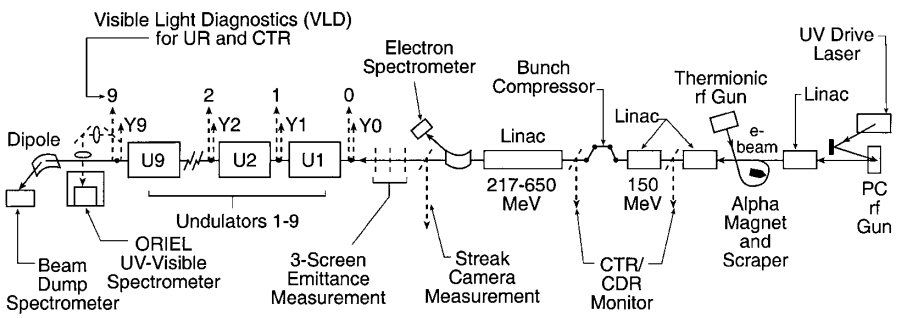

FIG. 1. A schematic of the experiment showing the PC gun, linac, bunch compressor, e-beam spectrometer, three-screen emittance station, nine undulators, the optical diagnostic stations, the UV-visible spectrometer, and the e-beam dump spectrometer.

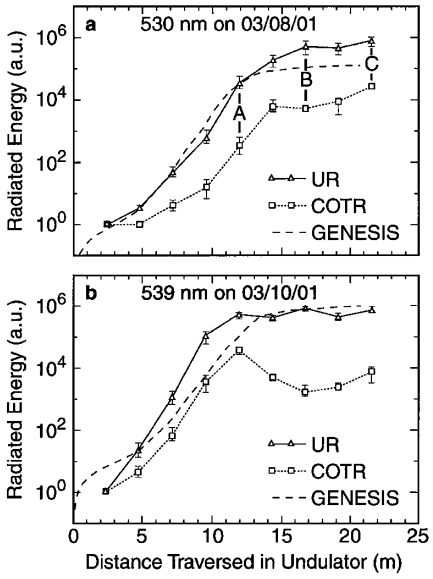

FIG. 2. The observed UR and COTR signal vs z position along the undulator series for (a) 530-nm run and (b) 539-nm run. The normalization point was at the exit of the first undulator (2.4 m) for all experimental curves. The GENESIS simulation results are shown as the dashed curves.

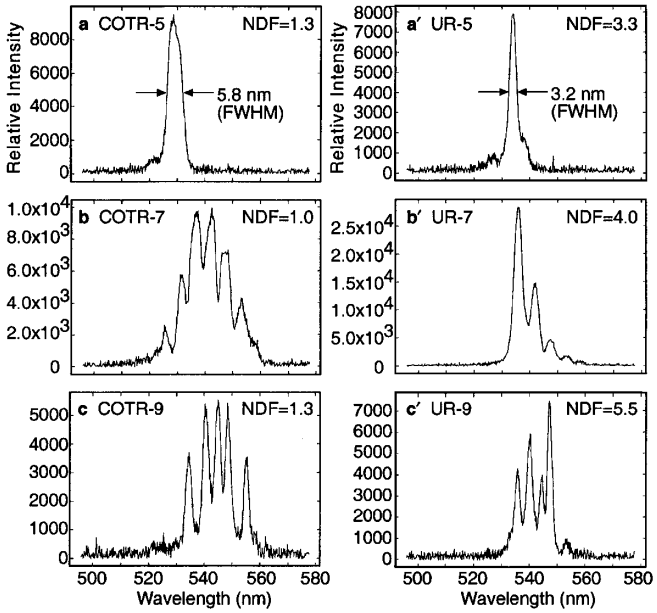

FIG. 3. A composite of the COTR spectra (a)–(c) and UR spectra (a′)–(c′) measured at positions A, B, and C in Fig. 2a (after U5, U7, and U9). The transition from simple spectra to the complex spectra with sidebands is seen in both columns. The neutral density filter (NDF) values are also indicated.

way to detect the critical change in the microbunching fraction at/after SASE saturation. We suggest that one key signature of saturation is indeed the peaking of the microbunching fraction (in this case, ~20%), which is more directly detected with the COTR-based techniques. The results of GENESIS [15] simulations based on the average of 50 different seeds are also plotted as the dashed line in both Figs. 2a and 2b. Reasonable agreement is seen in Fig. 2a, but the data of Fig. 2b show a higher initial gain than the simulation. The simulation was matched at the 4.8-m point in both cases.

In addition, for the first time we tracked the COTR spectral evolution from the exponential gain regime into the saturation regime. The results are shown in Fig. 3 along with the UR spectra. In the exponential gain regime (point A in Fig. 2a) the observed spectrum is a single, narrow peak in Figs. 3a and 3a′ with 5.8- and 3.2-nm (FWHM) widths, respectively. After saturation (points B and C in Fig. 2a), the spectra are more complex (spectral width 5%). A mix of both regularly spaced (~4–6 nm apart) spectral lines and chaotic spectral intensities is seen in both the COTR and UR spectra for U7 and U9. Again these data are from a single micropulse and are an example from 100 samples. We are not aware of reports of such spectra for SASE experiments in the literature. These spectral features are reminiscent of those seen in some FEL oscillator experiments of the late 1980s [16], where the increase in optical power with a pass number is analogous to the increase in optical power with z in SASE. Moreover, evaluations of the full 2D images of x-λ space show a clear x dependence of COTR spectral centroid (~1.4-nm slew) at U5 and of COTR spectral structure in U7 and U9 data. We also operated at a much lower peak current (70 A) on the same night and observed simple spectral lines [1.8 nm (FWHM)] after U8. This shows that our optical transport was not the source of the observed spectral complexity. The proposed spiking of FEL oscillator optical pulses and similar spiking in z within the micropulse obtained from the results of GENESIS [15] and GINGER [17] SASE simulations lead us to expect discrete lies in the spectra. In both simulations the line spacing generated was about 2–3 nm, and regular order was not seen. Using a standard synchrotron sideband model with our estimated optical field peak power of 10^{13} W/m^2, we calculated a spacing of 4.9 nm, which is consistent with the experimental spacing of 4–6 nm.

To this point we have discussed only the integrated intensity result from the z-dependent COTR far-field images (see Fig. 2). Figure 4 is a COTR interferometer (COTRI) angular distribution image that actually contains a wealth of diagnostic information. Recall that when the thin foil is inserted at a station, it both blocks the strong SASE light and combines with the 45° pickoff mirror to provide the two COTR sources that interfere to form the interferogram. This image, taken after the eighth undulator ($z = 19.2$ m) for the 539-nm case, has an integrated intensity that is 10 to 20 times weaker than the 12.5-m saturation point, so the bunching fraction has decreased by approximately the square root of that ratio. However, the θ_x-θ_y asymmetry, the $\pm\theta_x$ and $\pm\theta_y$ symmetry, and the outer fringe visibility when viewed in light of our analytical model [9] involve additional physics. The θ_x-θ_y asymmetry is readily explained as being due to the e-beam's asymmetric beam shape ($\beta_x = 2.7$ m, $\beta_y = 0.7$ m) and its interaction with the SASE optical fields. The nominal e-beam sizes for a

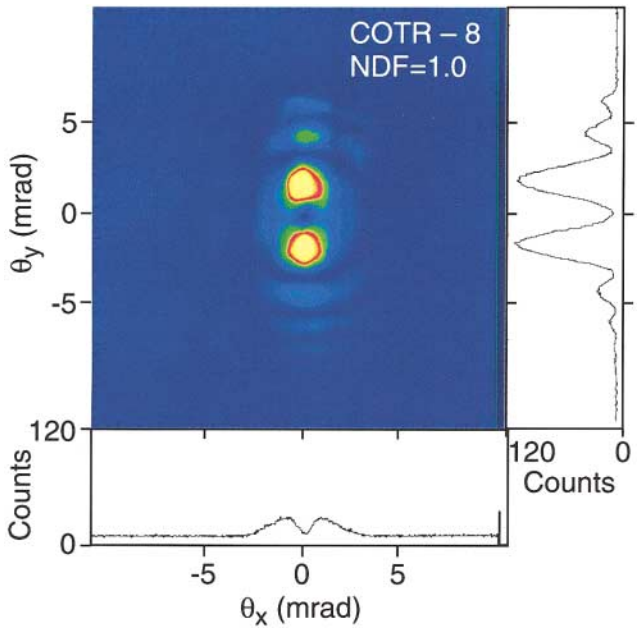

FIG. 4 (color). COTRI angular distribution image after undulator 8 showing the central lobes in θ_x-θ_y space and the profiles for θ_x and θ_y, below and to the right of the image, respectively. The visibilities of the second and third fringe maxima are consistent with a "core" of beam with $\sigma_y \approx 30$ μm that is still microbunched. The image colors blue, green, red, and yellow go from low to high intensity.

matched beam are $\sigma_x \approx 200$ μm and $\sigma_y \approx 100$ μm. The corresponding bunch form factors from Eq. (2) result in a larger product intensity for vertical angles, hence this basic COTRI image asymmetry. The fact that the $\pm\theta_x$ and $\pm\theta_y$ lobe intensities are similar implies that the effective electron-beam distributions in x and y are each symmetric and the beam is well centered. The outer fringe visibility is related to two effects. First, the OTRI fringe pattern for the single-electron case is dependent on a convolution with the beam divergence in the model, and we have found that a beam divergence of $\sigma_{y'} = 0.2$ mrad is consistent with the data. Second, the very presence of COTRI outer fringes indicates that there is an effective "beam size" feature that is less than 50 μm. In particular, the Fig. 4 data exhibit three (four) fringes at $\pm\theta_y$ values whose relative intensities are 1.0, 0.24, 0.12, and (0.04), and the calculated ones are 1.0, 0.24, 0.13, and (0.04) using $\sigma_y = 30$ μm in the model. The fringe maxima are at $\theta_y = \pm 1.8$, 4.5, and 6.3 mrad and within 5% of the calculated ones. The single horizontal lobes, with the almost linear ramp shape on the outer θ_x side, are consistent with $\sigma_x \approx 80$–120 μm. In both planes then, the COTRI image indicates an "effective" size or feature 2–3 times smaller than the expected e-beam total size. A similar residual microbunched core after some debunching outside the wiggler was previously reported in an FEL amplifier experiment [18].

In summary, we have extended our verification of the electron-beam bunching fraction evolution using COTR along the undulators in a SASE FEL experiment to the saturated regime. We have reported for the first time evidence of synchrotron sidebands in the microbunching, a peaking of the microbunching fraction near saturation, and evidence of an effective transverse core involved in the microbunching and x dependence of the microbunching spectrum. These features have been compared to calculations using GENESIS and GINGER where possible. An improved understanding of the SASE process has resulted, since the COTR techniques provide a unique probe of the critical microbunching phenomenon.

The authors acknowledge discussions with W. Fawley (LBNL) and N. Vinokurov (Budker Institute) and the support of P. Den Hartog, O. Singh, G. Decker, A. V. Rauchas, E. Gluskin, R. Gerig, and J. N. Galayda (all of the Advanced Photon Source). The work of the Argonne authors is supported by the U.S. Department of Energy, Office of Basic Energy Sciences, under Contract No. W-31-109-ENG-38.

*Also at Max-Laboratory, Lund, Sweden S-22100.
†Present address: Carderock Division, NSWC, West Bethesda, Maryland 20817.

[1] C. Pellegrini, Nucl. Instrum. Methods Phys. Res., Sect. A **475**, 1 (2001), and references therein.
[2] Y. S. Derbenev, A. M. Kondratenko, and E. L. Saldin, Nucl. Instrum. Methods Phys. Res., Sect. A **193**, 452 (1982).
[3] R. Bonifacio, C. Pellegrini, and L. Narducci, Opt. Commun. **50**, 373 (1984).
[4] K.-J. Kim, Nucl. Instrum. Methods Phys. Res., Sect. A **250**, 396 (1986); J.-M. Wang and L. H. Yu, Nucl. Instrum. Methods Phys. Res., Sect. A **250**, 484 (1986).
[5] A. H. Lumpkin *et al.,* Phys. Rev. Lett. **86**, 79 (2001).
[6] S. V. Milton *et al.,* Science **292**, 2037 (2001).
[7] R. A. Jong, E. T. Scharlemann, and W. M. Fawley, Nucl. Instrum. Methods Phys. Res., Sect. A **272**, 99 (1988).
[8] L. Wartski *et al.,* J. Appl. Phys. **46**, 3644 (1975).
[9] D. W. Rule and A. H. Lumpkin, in *Proceedings of the 2001 Particle Accelerator Conference* (IEEE, Piscataway, NJ, 2001), pp. 1288–1290.
[10] A. Tremaine *et al.,* Phys. Rev. Lett. **81**, 5816 (1998).
[11] S. Biedron *et al.,* in *Proceedings of the 1999 Particle Accelerator Conference* (IEEE, Piscataway, NJ, 1999), p. 2024.
[12] M. Borland, J. Lewellen, and S. V. Milton, in *Proceedings of the XX Linac Accelerator Conference* (e Conf, Menlo Park, CA, 2000), p. 863.
[13] E. Gluskin *et al.,* Nucl. Instrum. Methods Phys. Res., Sect. A **429**, 358 (1999).
[14] A. H. Lumpkin *et al.,* Nucl. Instrum. Methods Phys. Res., Sect. A **296**, 150 (1990); D. W. Rule *et al.,* Nucl. Instrum. Methods. Phys. Res., Sect. A **296**, 739 (1990).
[15] S. Reiche, Nucl. Instrum. Methods Phys. Res., Sect. A **429**, 243 (1999).
[16] R. W. Warren *et al.,* Nucl. Instrum. Methods Phys. Res., Sect. A **285**, 1 (1989).
[17] W. Fawley, BP Tech Note-104, Lawrence Berkeley Laboratory, 1995).
[18] J. Gardelle, J. Labrouche, and J. L. Rullier, Phys. Rev. Lett. **76**, 4532 (1996).